CHEMISTRY OF MATERIALS

Article

pubs.acs.org/cm

Using Machine Learning To Identify Factors That Govern Amorphization of Irradiated Pyrochlores

Ghanshyam Pilania,[†] Karl R. Whittle,[‡] Chao Jiang,[§] Robin W. Grimes,[∥] Christopher R. Stanek,[†] Kurt E. Sickafus,[⊥] and Blas Pedro Uberuaga*[,†]

[†]Materials Science and Technology Division, Los Alamos National Laboratory, Los Alamos, New Mexico 87545, United States
[‡]School of Engineering, University of Liverpool, Liverpool L69 3BX, United Kingdom
[§]Fuels Modeling and Simulation Department, Idaho National Laboratory, Idaho Falls, Idaho 83415, United States
[∥]Department of Materials, Imperial College London, London SW7 2AZ, United Kingdom
[⊥]Department of Materials Science and Engineering, University of Tennessee, Knoxville, Tennessee 37996, United States

Supporting Information

ABSTRACT: Structure−property relationships are a key materials science concept that enables the design of new materials. In the case of materials for application in radiation environments, correlating radiation tolerance with fundamental structural features of a material enables materials discovery. Here, we use a machine learning model to examine the factors that govern amorphization resistance in the complex oxide pyrochlore ($A_2B_2O_7$) in a regime in which amorphization occurs as a consequence of defect accumulation. We examine the fidelity of predictions based on cation radii and electronegativities, the oxygen positional parameter, and the energetics of disordering and amorphizing the material. No one factor alone adequately predicts amorphization resistance. We find that when multiple families of pyrochlores (with different B cations) are considered, radii and electronegativities provide the best prediction, but when the machine learning model is restricted to only the B = Ti pyrochlores, the energetics of disordering and amorphization are critical factors. We discuss how these static quantities provide insight into an inherently kinetic property such as amorphization resistance at finite temperature. This work provides new insight into the factors that govern the amorphization susceptibility and highlights the ability of machine learning approaches to generate that insight.

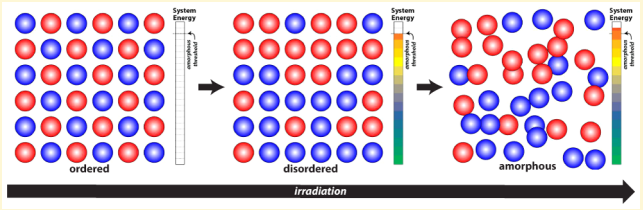

INTRODUCTION

Designing materials for advanced or next-generation applications requires understanding how properties are related to structure, that is, identifying so-called structure−property relationships. Having such relationships guides the search for new materials with enhanced performance by identifying regions of structure and composition space that exhibit superior properties. For nuclear energy materials, a key performance metric is tolerance against radiation damage. Pyrochlores ($A_2B_2O_7$) have been extensively studied for their potential application as nuclear waste forms[1−10] and have been incorporated into some compositions of the SYNROC waste form.[11] In this context, significant effort has been directed toward understanding how the chemistry of the pyrochlore, the nature of the A and B cations, dictates the amorphization susceptibility of the compound. In particular, several experimental efforts[12−16] have been focused on determining the critical amorphization temperature, T_C, the temperature at which the material recovery rate is equal to or faster than the rate of damage, as summarized in Figure 1. Typically, these experiments were performed in an electron microscope equipped with an ion source, such that samples were simultaneously irradiated with electrons and 1 MeV Kr ions. Though the value of T_C varies with ion irradiation conditions,[17] 1 MeV Kr ion irradiation results should be comparable and thus provide a common reference for comparing susceptibility to amorphization of chemically distinct compounds.

As a consequence, a number of "features", or basic structural and energetic properties, have been identified that provide insight into the radiation response of pyrochlores. These include the radii and electronegativities of the A and B cations;[8,13] the x parameter, which describes how the oxygen sublattice deviates from ideality;[4,8,13] the enthalpy of formation of the pyrochlore;[6,18] and the energy to disorder the pyrochlore to a disordered fluorite structure.[1,19] Further, there has been discussion on the extent of the disordered phase field in the phase diagram and its relationship to amorphization resistance.[7] Most of these features have been only heuristically correlated with amorphization resistance or only applied to a subset of pyrochlore chemistries. We are only aware of one attempt to

Special Issue: Computational Design of Functional Materials

Received: November 1, 2016
Revised: February 9, 2017
Published: February 10, 2017

DOI: 10.1021/acs.chemmater.6b04666
Chem. Mater. 2017, 29, 2574−2583

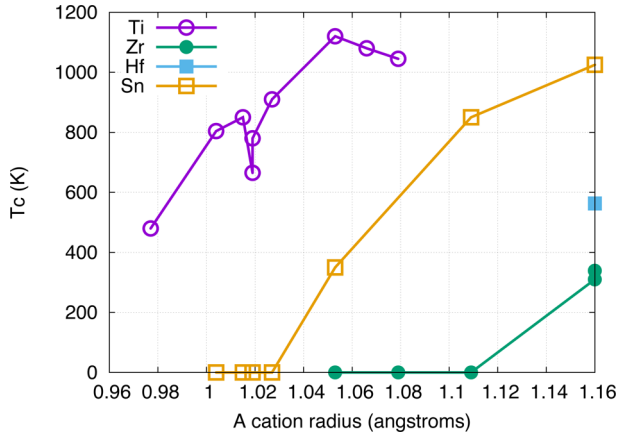

Figure 1. Experimentally measured values of T_C, ordered as a function of A cation radius, for several different pyrochlores. All of these values of T_C were obtained for 1 MeV Kr irradiations. Compounds for which amorphization has not been observed are plotted here as having T_C = 0 K. Data from refs 12−16.

quantify the relationship between these types of features and a prediction of T_C. In that work, Lumpkin and co-workers established a relationship between T_C and lattice constants, electronegativities, disordering energetics, and oxygen positional parameter.[8] While their model provided a significant advance in describing the structure−property relationships of pyrochlores, here we demonstrate how, through the use of machine learning, greater insight can be extracted. In particular, while they considered the disordering energy as one of their features, they used data from atomistic potentials that does not adequately describe all of the chemistries in the experiments. Further, they did not have access to data describing the amorphous state of these compounds. Finally, modern machine learning methods, applied to materials science, offer new avenues to examine the structure−property relationships in these types of systems.

Here, we use machine learning methods to demonstrate how a set of features, for a range of pyrochlore chemistries, can be used to predict T_C. We use both structural parameters such as cation radius and electronegativity supplemented by energetics calculated with density functional theory (DFT) to build a database of features as a function of pyrochlore chemistry. We analyze this database, building machine learning models that predict T_C as a function of pyrochlore chemistry based on a systematic collection of features. We consider pyrochlore chemistries for which experimental data exists for T_C, which includes pyrochlores where B = Ti, Zr, Hf, and Sn. [Here, and in what follows, when we refer to the B cation, we mean the B chemistry of the pyrochlore (the nature of the 4+ species).] We find that, when considering the full range of chemistries, the two features that best predict T_C are the ratio of the radii and the difference in electronegativities of the A and B cations. However, to predict more subtle dependencies of T_C with pyrochlore chemistry characteristic of a given B chemistry, the energies to disorder and amorphize the compound provide a better prediction of T_C. Importantly, the energy to disorder the compound alone does not correlate with T_C and must be complemented by information about the energy to amorphize the material.

As compared to Ti, Hf, or Zr, Sn is a chemically very different element. It, like Ti, is multivalent, but unlike Ti, it has a much stronger prevalence to adopt a charge state other than 4+. Further, as discussed below, it has a significantly higher electronegativity than the other B cations, producing a more covalent bond. This implies that Sn pyrochlores should be less amorphization resistant.[20] However, experiments have shown Sn pyrochlores to be more amorphization resistant than other pyrochlores.[5] This all suggests that Sn pyrochlores are electronically much more complex than the other pyrochlore families, which is one reason that we use DFT to determine the energetics of disordering and amorphization, as DFT can account for the varied valence of the Sn cations. Further, the inclusion of Sn pyrochlores in this analysis, precisely because the behavior is counterintuitive, provides a more stringent test of the methodology.

It is important to emphasize that, in this paper, we are regarding T_C as a metric that correlates with the relative amorphization resistance of different compounds. As discussed below, T_C is not an intrinsic property of a material, but depends on external factors such as irradiation conditions. In particular, the mechanism of amorphization changes with irradiation conditions.[21] Our analysis pertains only to irradiation conditions in which amorphization proceeds via a defect accumulation mechanism. T_C is also a complicated function of material properties. Thus, actually predicting T_C for a given compound and irradiation condition is extremely challenging. However, differences in T_C are expected to indicate how easily one compound can be amorphized compared to another. By correlating material features with T_C, we provide direct insight into what features dictate amorphization resistance.

METHODOLOGY

Density Functional Theory. Density functional theory (DFT) calculations were performed using the all-electron projector augmented wave method[22] within the generalized gradient approximation (PBE) with the VASP code.[23] A plane-wave cutoff of 400 eV and dense *k*-point meshes were used to ensure convergence. The lattice parameters and all atomic positions were allowed to relax, though the cells were constrained to be cubic. The disordered fluorite structure was modeled using the special quasirandom structures (SQS) approach.[24] The SQS structures were generated as described in ref 25. The amorphous structures were created by performing *ab initio* molecular dynamics at a very high temperature and then quenching the structures to 0 K. For the B = Zr and Hf families, there is a deviation from true monotonic behavior at A = Tb, in contrast with previous DFT calculations[25] that used the same methodology (pseudopotentials, functional, *k*-point mesh, and energy cutoff). We assume that the differences from previously published results are due to changes in different versions of VASP. Finally, we use the so-called "f-in-core" approach for the 3+ A cations, in which the f electrons are not treated explicitly but are placed in the core of the pseudopotential. Thus, while experimental data for T_C exists for $Yb_2Ti_2O_7$, we do not consider it here as such pseudopotentials do not exist for Yb in VASP.

Machine Learning Model. We used Kernel ridge regression (KRR) with a Gaussian kernel for machine learning, using the Scikit-learn machine learning suite.[26] KRR is a similarity-based learning algorithm, which has recently been very successful for a range of materials property prediction problems. Some recent applications of this approach to materials problems include predictions of the properties of molecular[27,28] and periodic systems,[29,30] development of adaptive force fields,[31,32] crystal structure classification,[33] dielectric breakdown strength prediction,[34,35] self-consistent

DOI: 10.1021/acs.chemmater.6b04666
Chem. Mater. 2017, 29, 2574−2583

solutions for quantum mechanics,[36] and predictions of bandgaps.[37] The treatment in this paper is, to the best of our knowledge, one of the first, along with ref 38, that uses machine learning to analyze a small experimental data set to build a predictive model.

Feature standardization was carried out by rescaling each individual feature such that it has a zero mean and unit variance before building the KRR model. Within KRR, the ML estimate of a target property (in our case the critical temperature T_C) of a new system j is estimated by a sum of weighted kernel functions (i.e., Gaussians) over the entire training set, as

$$T_{Cj}^{\mathrm{ML}} = \sum_{i=1}^{N} w_i \exp\left(-\frac{1}{2\sigma^2}|\mathbf{d}^{ij}|^2\right) \quad (1)$$

where i runs over the systems in the training data set, and $|\mathbf{d}^{ij}|^2 = \|\mathbf{d}_i - \mathbf{d}_j\|_2^2$, the squared Euclidean distance between the feature vectors $\mathbf{d}_i$ and $\mathbf{d}_j$. The coefficients w_i's are obtained from the training (or learning) process built on minimizing the expression $\sum_{i=1}^{N}(T_{Ci}^{\mathrm{ML}} - T_{Ci}^{\mathrm{Exp}})^2 + \lambda \sum_{i=1}^{N} w_i^2$, with T_{Ci}^{ML} being the ML estimated critical temperature and T_{Ci}^{Exp} being the corresponding experimental value, and the model hyperparameters σ and λ are optimized within a internal cross-validation loop. The explicit solution to this minimization problem is $\boldsymbol{\alpha} = (\mathbf{K} + \lambda\mathbf{I})^{-1}\mathbf{T}_C^{\mathrm{Exp}}$, where $\mathbf{I}$ is the identity matrix, and $K_{ij} = \exp\left(-\frac{1}{2\sigma^2}|\mathbf{d}^{ij}|^2\right)$ are the kernel matrix elements of all materials in the training set. The parameters λ and σ are determined in an inner loop of 5-fold cross-validation using a logarithmically scaled fine grid.

RESULTS

DFT Energetics. Figure 2a provides the energetics for disorder and amorphization of a given pyrochlore, as found using DFT, as a function of the chemistry of the pyrochlore. These are ordered by A cation radius. Focusing first on the energetics to disorder, there is a general trend that as the A cation radius increases, the energy associated with disordering the pyrochlore to a disordered fluorite also increases, consistent with previous results using DFT.[25] This is particularly true of the B = Zr, Hf, and Sn families of pyrochlores. For the B = Ti family, there is a peak in the disorder energy near the A = Gd composition, again consistent with previous DFT and empirical potential calculations.[19,25]

Figure 2a highlights the apparent contradiction between experimental observations and the notion that the disordering energy correlates with amorphization resistance. If only disordering energetics dictated the response of the pyrochlore to irradiation, then one would expect that Zr pyrochlores would generally exhibit higher amorphization resistance than Ti pyrochlores (which they do) but also that Sn pyrochlores would be less resistant to amorphization than Ti pyrochlores, which they are not. Thus, other factors must also be important. We propose that the energy of the amorphous phase is one of those factors.

The energy differences between ordered pyrochlore and an amorphous structure are also provided in Figure 2a. In the case of the B = Hf and Zr families, these are again relatively monotonic with increasing A cation radius. However, the behaviors of the B = Ti and Sn families are more complex. In particular, for the B = Ti family, the amorphous energy is nonmonotonic with A cation radius, but the peak is for a different chemistry than was the disordering energy. In the B = Ti family, the amorphous energy is greatest for A = Y and generally is high for A = Dy and Tb. The B = Sn family exhibits even more complicated behavior. There is a peak in the amorphous energy for A = Gd and a minimum for A = Ho.

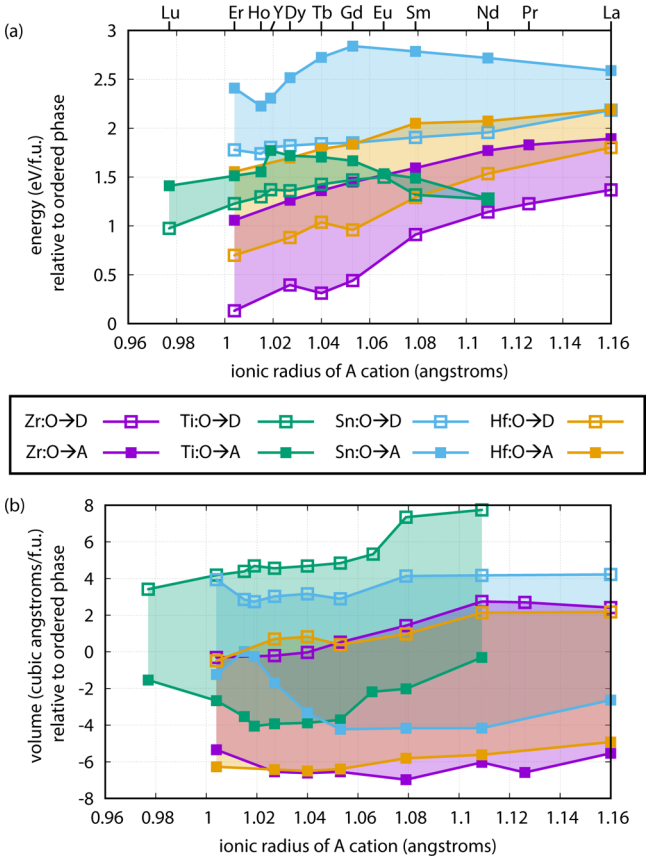

Figure 2. DFT results for the (a) energetics and (b) volume changes associated with an order-to-disorder (O → D, open symbols) and an order-to-amorphous (O → A, closed symbols) transformation for four families of pyrochlores in which B = Ti (green), Zr (purple), Hf (yellow), and Sn (cyan). The shaded regions highlight the differences between the disordered and amorphous structures.

Finally, the shaded regions in Figure 2a highlight the energy gap between the disordered and amorphous states. The variation of this gap with A cation radius is very different for the different families of pyrochlores. For the B = Zr and Hf pyrochlores, the gap slowly but steadily decreases with A cation radius. For the B = Ti pyrochlores, the gap first increases slightly and then decreases to essentially zero for the A = Nd chemistry. The gap for the B = Sn pyrochlores first decreases, then increases, and then decreases again. Further, the gap is smallest for the B = Ti pyrochlores and, overall, largest for the B = Zr and Sn pyrochlores, at least for some A chemistries.

Figure 2b provides the volume changes between the ordered phase and both the disordered and amorphous phases, as determined from the DFT calculations. For nearly all of the cases, a transformation from the ordered to disordered phase results in a volume expansion while the formation of the amorphous phase contracts the lattice. The exceptions are the B = Zr and Hf pyrochlores with small A cations, which exhibit very little change in volume upon disordering. On the other hand, $Nd_2Ti_2O_7$ (assumed to be cubic here), $Y_2Sn_2O_7$, and $Ho_2Sn_2O_7$ exhibit very little change upon amorphization.

DOI: 10.1021/acs.chemmater.6b04666
Chem. Mater. 2017, 29, 2574−2583

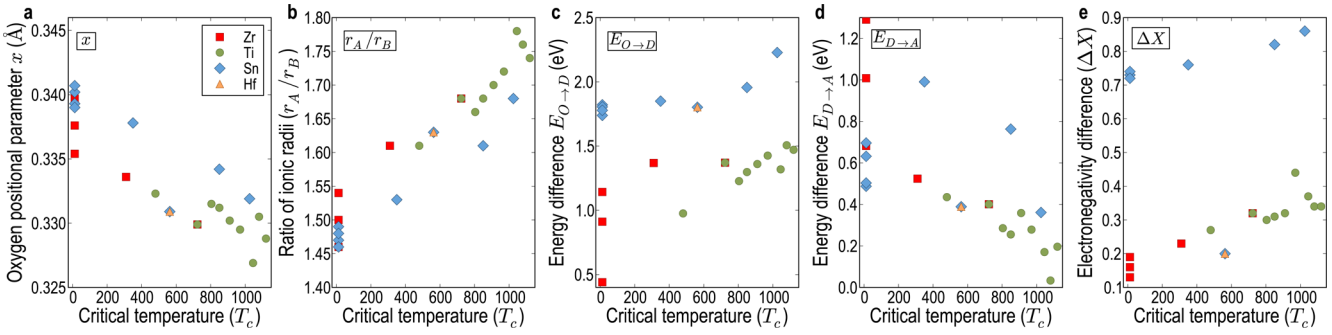

Figure 3. Correlations between experimental measurements of T_C and 5 features describing pyrochlores. (a) x, the oxygen positional parameter (x = 0.375 for perfect fluorite). (b) r_A/r_B, the ratio of cation radii. (c) $E_{O\to D}$, the energy difference between disordered fluorite and ordered pyrochlore. (d) $E_{D\to A}$, the energy difference between an amorphous structure and disordered fluorite. (e) ΔX, the difference in electronegativity between the A and B cation. The different symbols in the figures indicate the nature of the B cation (■ = Zr, ● = Ti, ◆ = Sn, ▲ = Hf).

Correlation of Features with Amorphization Resistance. The DFT results reveal that there are significant differences in the energetics of disorder and amorphization in pyrochlores as a function of both A and B chemistry. We use a machine learning approach to quantify the correlations between these energetics, as well as other features associated with pyrochlores, and the amorphization resistance, as characterized by T_C. The features considered here are r_A/r_B, the ratio of the ionic radii of the A and B cations; $\Delta X = X_B - X_A$, the difference in electronegativity of the A and B neutral metal atoms (X_A and X_B, respectively); x, the oxygen positional parameter, which measures the deviation of the oxygen sublattice from an ideal (fluorite-like) simple cubic sublattice; $E_{O\to D}$, the energy difference between the disordered and ordered phases; and $E_{D\to A}$, the energy difference between the amorphous and disordered phases. All of the values used are summarized in Table S1 in the Supporting Information. These features were chosen because (a) they have been shown to correlate to some degree in previous studies and (b) our DFT results indicate that the energetics depend strongly on the A and B chemistry of the pyrochlore, suggesting they may provide a strong descriptor of each compound. We also considered the enthalpy of formation, proposed by other authors as a factor in radiation tolerance,[6,18] calculated here with DFT, but found that it did not lead to any improvement in the description of T_C or any change in the conclusions reached here, and so is not discussed further here.

However, before we examine the results of the machine learning model, it is instructive to examine how the selected features correlate with T_C. Figure 3 provides simple plots of each feature against T_C. The values for T_C, summarized in Table 1, are taken from refs 12−16. For all of these values of T_C, the irradiations were performed with 1 MeV Kr ions under the same conditions at the same facility. Figure 3 reveals that while there are rough correlations between T_C and some of the features, there is not one feature that provides a quantitative capability of predicting T_C (a result that will be quantified below). For example, overall, r_A/r_B correlates well with T_C over a wide range of B chemistries; however, it does not capture subtleties associated with variations in T_C with a given family of pyrochlores. ΔX, on the other hand, discriminates between pyrochlores with B = Sn and the other families but does not correlate directly with T_C. Similarly, x shows an overall correlation with T_C, but again, the details are lost. $E_{O\to D}$, on the other hand, seems to correlate reasonably well for pyrochlores within a given family but does not describe variations of T_C between families. Finally, $E_{D\to A}$, similar to x and ΔX, seems to generally correlate separately for B = Sn pyrochlores and the other families of pyrochlores. Thus, while there are rough trends indicating some insight from each of these features, there is certainly not enough of a correlation in any case for a quantitative prediction. However, this suggests, as noted by other authors,[8] that combinations of these features

Table 1. Values of T_C Used in the Machine Learning Model[a]

compd	T_C (K)	error (K)	ref
$Sm_2Ti_2O_7$	1045	n/a	12
$Eu_2Ti_2O_7$	1080	n/a	12
$Gd_2Ti_2O_7$	1120	n/a	12
$Tb_2Ti_2O_7$	970	n/a	12
$Dy_2Ti_2O_7$	910	n/a	12
$Y_2Ti_2O_7$*	780	n/a	12
$Y_2Ti_2O_7$*	665	33	15
$Ho_2Ti_2O_7$	850	n/a	12
$Er_2Ti_2O_7$	804	n/a	12
$Lu_2Ti_2O_7$	480	n/a	12
$La_2Zr_2O_7$†	339	49	13
$La_2Zr_2O_7$†	310	n/a	12
$Nd_2Zr_2O_7$	<25	n/a	12
$Sm_2Zr_2O_7$	<25	n/a	12
$Gd_2Zr_2O_7$	<25	n/a	12
$La_2Hf_2O_7$	563	22	13
$La_2Sn_2O_7$	1025	n/a	12
$Nd_2Sn_2O_7$	850	n/a	12
$Gd_2Sn_2O_7$	350	n/a	12
$Dy_2Sn_2O_7$	<25	n/a	12
$Ho_2Sn_2O_7$	<25	n/a	12
$Y_2Sn_2O_7$	<25	n/a	12
$Y_2Sn_2O_7$	<50	n/a	14
$Er_2Sn_2O_7$	<25	n/a	12

[a]As reported by the corresponding references. The corresponding irradiation conditions were 1 MeV Kr in all cases. In the case of $Y_2Ti_2O_7$ (*), as there were two significantly different values in the literature, we took an average value of T_C: 723 K. In the case of $La_2Zr_2O_7$ (†), there were also two literature values, but as one was within the error bars of the other, we simply took T_C = 310 K for this compound. The error bars were not used in the machine learning model as, owing to the limited data, ML models never reached accuracies where the error bars were relevant. For those compounds where no T_C was measured (i.e., T_C < 25 K), we simply used a value of T_C = 12.5 K for numerical reasons.

DOI: 10.1021/acs.chemmater.6b04666
Chem. Mater. 2017, 29, 2574−2583

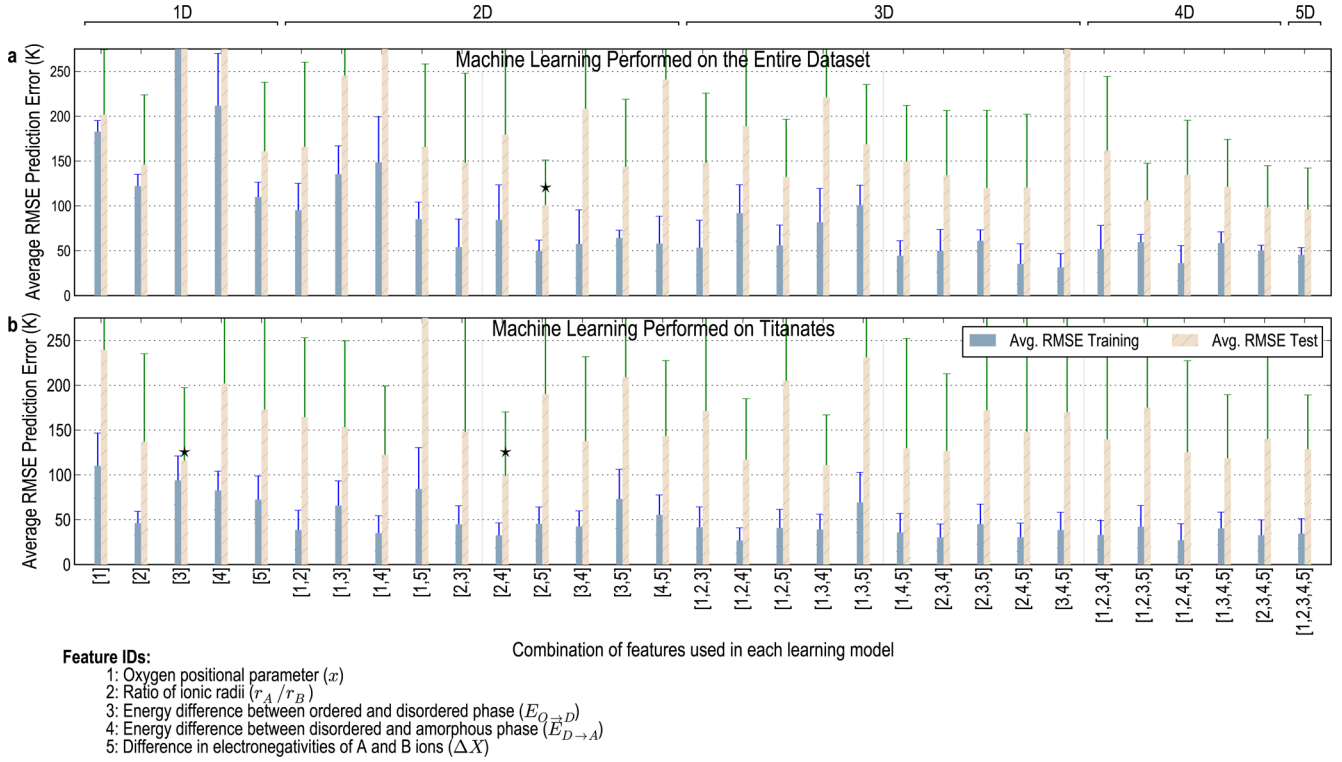

Figure 4. Results from the machine learning model. (a) Results when applied to the entire set of pyrochlores and (b) results when applied only to the titanate family. The solid bars indicate the average RMS error for the training data while the hashed bars indicate the error for the test data. The indices on the abscissa indicate the features used in that particular model. Models including 1, 2, 3, 4, or all 5 features were considered. The best 2D feature set is indicated with the star for both cases. Error bars represent the standard deviations for the RMSE in predict T_C, computed over the 100 different training/test set splits.

may provide predictive capability. Hence, we use a machine learning approach to quantify this.

Results of the Machine Learning Model. We use a machine learning (ML) approach to quantify the correlations between the five features described in the previous section and T_C. More specifically, we employed kernel ridge regression (KRR),[39−41] an algorithm that works on the principle of similarity and is capable of extracting complex nonlinear relationships from data in an efficient manner, with a Gaussian kernel to learn and quantify trends exhibited by T_C in the feature space discussed above. A randomly selected 90%/10% training/test split of the available data was used for statistical learning and testing the performance of the trained model on previously unseen data. A leave-one-out cross-validation is used to determine the model hyperparameters to avoid any overfitting of the training data that may lead to poor generalizability. The trained model can subsequently be used to make an interpolative prediction of T_C for a new material (i.e., not used in the model training) i by comparing its distance in feature space d_i (suitably defined by a distance measure; in our case the Euclidean norm was used) with those of a set of reference training cases for which the T_C values are known. Further details of our KRR-based ML models are provided in the Methodology section.

Next, within the KRR ML model, we aim to identify the best feature combination that exhibits the highest prediction performance, quantified by its ability to accurately predict T_C of the test set compounds. We do this in a comprehensive manner by building KRR ML models using all possible combinations of Ω features with $\Omega \in [2, 5]$. Performance of each of these models was evaluated separately on the entire data set as well as on a reduced set that only included the Ti pyrochlores. The root-mean-square errors (RMSEs) for the T_C predictions on training and test sets for various models are presented in Figure 4. In order to account for model prediction variability associated with randomly selected training/test splits, Figure 4 reports the RMSEs averaged over 100 different randomly selected training/test splits for each of the models. The average of the RMSE on the test set quantifies the predictive capability of the model and thus is used to identify the features that best describe the experimental data.

Figure 4 provides the results of the machine learning model when different dimensionalities of feature sets are considered both for a database containing all of the pyrochlores from Table 1 and a database containing only the titanates (B = Ti). We first consider the results of using only one feature to train the model. As discussed above in the context of Figure 3, in the case of the full data set, none of the models based on one feature alone perform particularly well. The best correlation is found for r_A/r_B, but even there the error is nearly 150 K. If only the titanates are considered, the best performing feature is $E_{O\rightarrow D}$, which has an error of less than 125 K (indicated as a "★" in Figure 4b). This indicates that the disordering energetics do correlate well with the observed values of T_C.

The 2D models that lead to the lowest RMSEs on the test set data have been marked with a "★" in Figure 4a (when taking the entire data) and Figure 4b (for the Ti pyrochlores). It is interesting to note that, for both cases, going beyond the best performing 2D models does not lead to a significant improvement in the model prediction performance. For instance, while the best binary feature pair (r_A/r_B, ΔX) leads to a test set RMSE of 101.2 K in T_C, the ML models built on

DOI: 10.1021/acs.chemmater.6b04666
Chem. Mater. 2017, 29, 2574−2583

the best 4D and 5D (taking all 5 features considered) feature vectors only result in nominal improvements leading to RMSEs of 98.3 and 95.9 K, respectively. Since, as a general rule, higher model complexity often leads to poor generalizability, in the case of a comparable prediction performance, a simpler model (i.e., built on a lower dimensional feature set) should always be preferred over a more complex one. Therefore, henceforth we focus our attention on the best performing 2D models.

The superior performance exhibited by the (r_A/r_B, ΔX) feature pair is not entirely unexpected and can be understood by looking at Figure 3b,e. As alluded to previously, while r_A/r_B helps capture the overall T_C trends among different chemistries, ΔX allows for an effective separation between different chemistries (especially, between the Sn-based compounds and rest of the data set), while still capturing relative T_C trends between these subgroups. The best performing feature pair for the titanate pyrochlores data set, however, is constituted by r_A/r_B and $E_{D\rightarrow A}$. Further, the best feature pair for the full data set, (r_A/r_B, ΔX), performs much more poorly on this subset, indicating that more physics is needed to describe the more strongly related compounds within a given B cation family. We note that if the analysis is limited to just the B = Sn family, the best 2D feature pair remains (r_A/r_B, ΔX).

While Figure 4 captures the average performance and variability (taken over 100 different runs) for our best performing 2D models (marked with a ★), in Figure 5a,b we present parity plots comparing the experimental T_C with the ML predictions using the best 2D descriptors found for the entire data set (Figure 5a) and the titanates (Figure 5b), respectively. In each case ~90% of the data set was used for training (plotted as ■) with the remaining for testing the model performance (plotted as ●). In each case, we used four different ML runs randomly selecting training and test set splits (depicted by different colors). It can be seen from the parity plots that our ML models can reasonably predict (within the error bars established in Figure 4) T_C over the entire data set. A couple of conclusions can be drawn from these plots. First, visually it can be seen that the model prediction performance is comparable for the training and test sets, indicating that there is no overfitting (a problem when a ML model performs very well on a training set but exhibits a poor performance on a test set). Second, despite their simplicity (given that we are only using a two-dimensional feature in each case), the ML models exhibit good predictive power and stability (predictions do not change drastically over different training/test splits). This highlights the robustness of the model.

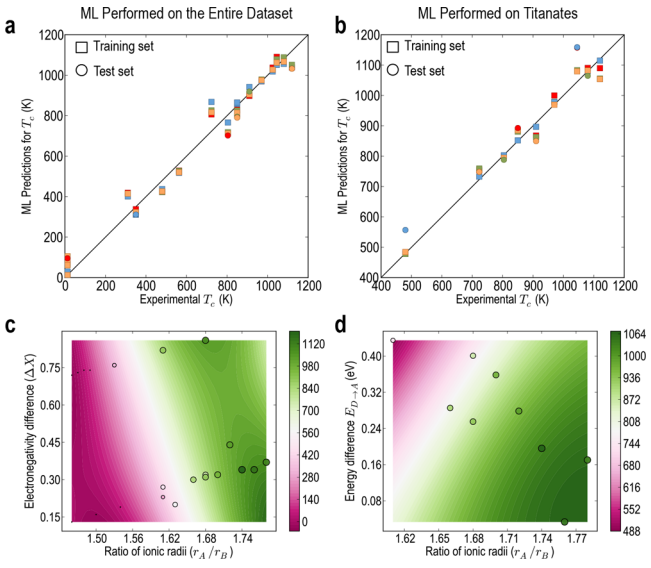

Figure 5. (a, b) Parity plots of the machine learning results for (a) the entire set of pyrochlores and (b) the titanate family. The squares represent training data while the circles are the test set. The different colors represent different runs with different training/test set splits. (c, d) Results from the machine learning model for (c) all of the pyrochlores considered and (d) just the titanate famliy. The size and color of the circles indicate the experimental T_C while the position of the circles indicates the predicted T_C. The contours indicate predictions of T_C for other values of the feature pairs.

To gain a deeper insight into the KRR model's prediction performance, we next construct contour plots for each of the two best performing 2D feature pairs discussed above. In each case, we start with a fine 2D grid in the feature space constituted by the primary features identified above, while still confining ourselves within the boundaries of the original feature space used to train the KRR models. Each point on this grid then, in principle, represents a point in the feature space, which can be used as an input for the respective trained KRR models to make predictions. That is, we map out the predicted value of T_C as a function of the two features over a range of values for each of the two features. Since the ML models are interpolative, one can readily use a fine grid in the 2D feature space to visualize trends in T_C versus the feature values and make predictions of T_C for new chemistries.

Figure 5c shows the best two-feature descriptor for the entire set of pyrochlores considered. Again, in this case, the two features that best correlate with T_C are r_A/r_B and ΔX. This combination of features is able to distinguish the different T_C behavior exhibited by the B = Sn pyrochlores and the other families of pyrochlores, by virtue of the properties of ΔX. In principle, the types of maps provided in Figure 5 could be used to predict T_C for chemistries of pyrochlores not included in Table 1. However, care must be taken as machine learning models are inherently interpolative in nature. Still, Figure 5c indicates that small r_A/r_B and small electronegativity differences between the A and B cations will maximize amorphization resistance (minimize T_C). Similarly, as shown in Figure 5d, minimizing r_A/r_B and maximizing $E_{D\rightarrow A}$ will also minimize T_C.

However, as discussed above, this combination of features has an effective uncertainty of ~100 K, indicating that it cannot describe the fine features exhibited by the B = Ti family of pyrochlores. For example, T_C is not monotonic with A cation radius (see Figure 1). As discussed, limiting the model to just the B = Ti pyrochlores results in a different optimal two-feature set, namely, r_A/r_B and $E_{D\rightarrow A}$, as shown in Figure 4b. In particular, as shown in Figure 5d, this set of features can describe the subtle behavior in which the A = Gd compound has the highest value of T_C, correlating with the fact that it has a relatively small value of $E_{D\rightarrow A}$, while the A = Y compound, which has a value of $E_{O\rightarrow D}$ similar to the neighboring compounds (see Figure 2a), exhibits an anomalously low value of T_C. This is a consequence of its rather high value of $E_{D\rightarrow A}$, a consequence of the fact that Y is not a rare earth, and thus, the bonding associated with it is subtly different to the other elements around it.

■ DISCUSSION AND CONCLUSIONS

Combining experimental results for T_C for various pyrochlore compounds, DFT calculations of the energetics of disordering

DOI: 10.1021/acs.chemmater.6b04666
Chem. Mater. 2017, 29, 2574−2583

and amorphization, and a machine learning model, we conclude that (a) basic ionic properties such as r_A/r_B and ΔX have the qualitative capability of predicting trends in T_C over a wide range of pyrochlore compounds but that (b) more quantitative predictions that capture the subtleties associated with variations in A cation chemistry require knowledge of both the disordering and amorphization energetics. This generalizes the previous understanding in which rough correlations between amorphization resistance and, for example, disordering energetics were hypothesized on the basis of a few observations.

However, what is clear from the machine learning analysis is that, even with the input of DFT energetics, the predictive capabilities are still limited. Even when limited to the B = Ti family of pyrochlores, the optimal 2D model results in predictive uncertainty of ∼100 K. This is a consequence of many factors, including the limited amount of experimental data, the uncertainties in the experimental data, and uncertainties in the DFT calculations. To determine an even better predictive model, more experimental data is required. In particular, values of T_C for other families of pyrochlores would enhance the strength of the model. For example, without the B = Sn pyrochlores, the importance of ΔX would likely not have been revealed. Importantly, given the small data set, domain knowledge, experience with the behavior of this system, was important in narrowing down a set of likely relevant features.

Inspection of Figure 2 shows that the compound $Eu_2Ti_2O_7$ does not quite follow the same trends in amorphization and disordering energies as its neighbors. In particular, it exhibits a very small difference in these two energies. The calculations for Eu used a different generation of pseudopotential than the other Ln^{3+} species and, because of this, may exhibit different behavior than the other Ln^{3+} compounds, which utilized an older generation of pseudopotential. Thus, one might suspect that the results for $Eu_2Ti_2O_7$ are an outlier. To test this, we redid the machine learning model on a database of titanates in which $Eu_2Ti_2O_7$ was not included; the results are presented in Figure 6. In this case, the best performing feature set is $E_{O\rightarrow D}$ and $E_{D\rightarrow A}$. Further, its performance is significantly better than the results of the model presented in Figure 4, with a predictive capability of better than 75 K. Further, the predictive error of the feature set that performed best on the full data set (r_A/r_B and ΔX) is the worst performing feature set on this data set. This highlights both the sensitivity of the model predictions when based on such small sets of data and the qualitatively different predictive capabilities of the approach depending on what type of data is included in the model.

While the feature set of ΔX and r_A/r_B has the best predictive capability for distinguishing between the various families of pyrochlores, the reason why Sn pyrochlores are radiation tolerant while exhibiting such high disordering energies is found in examining the amorphization energetics. The gap between the disordering and amorphization energies for the Sn pyrochlores is typically quite large, and even if, during the course of irradiation, enough energy is deposited into the lattice such that the structure becomes disordered, it is not enough to amorphize the material. The gap betwen the disordering and amorphization energies is much larger in the Sn pyrochlores than it is in the Ti family and, for some A cations, larger than for the Hf and Zr families as well. Thus, the origin of the radiation tolerance of some of the Sn pyrochlores comes from the fact that they are extremely difficult to amorphize. Importantly, by incorporating properties such as $E_{O\rightarrow D}$ and $E_{D\rightarrow A}$ that are derived from electronic structure calculations,

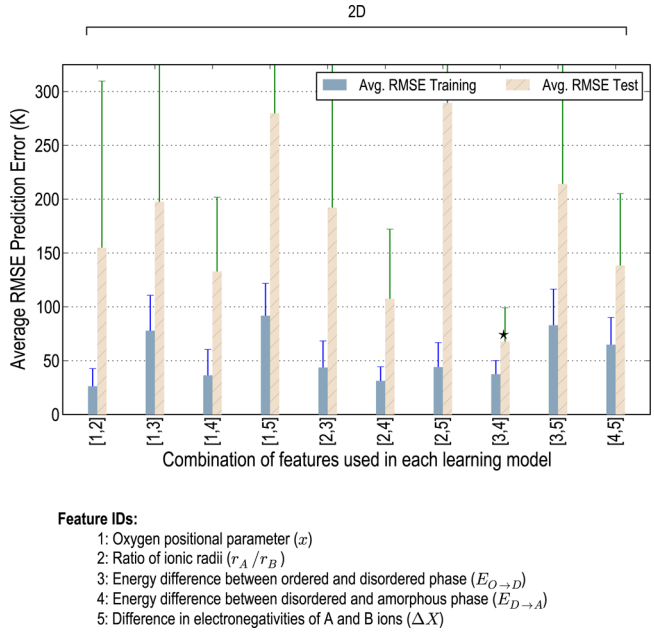

Figure 6. Results from the machine learning model on the titanate pyrochlores when $Eu_2Ti_2O_7$ is not included. Only results for 2D feature sets are shown. The best performing feature set is indicated by the star.

information about bonding in different environments (e.g., ordered, disordered and amorphous) is naturally included in the model. As noted, the behavior of the B = Sn pyrochlores is counterintuitive as it is typically assumed that higher levels of covalency leads to less amorphization resistance.[20] While the DFT results indicate that the energy to amorphize the Sn pyrochlores is extremely high, that fact does not provide a more fundamental explanation for this counterintuitive behavior. We suspect that there is such a high exothermic thermodynamic driving force to reorder that the barriers to recover from any damage are relatively small, as implied by the Bell−Evans−Polanyi principle[42,43] and similar to the effects we found in spinels.[44] This suggests that, while structural rigidity in the terms of strongly preferred coordination environments is typically detrimental to radiation tolerance,[20] extreme rigidity in coordination may provide some benefit. Recent results found that the amorphization resistance of Sn pyrochlores under swift heavy ion irradiation conditions did not seem strongly influenced by the covalency of the Sn−O bond.[45] However, our results suggests that this covalency, which does penalize disordering processes, further penalizes the amorphization of the Sn compounds, explaining the higher amorphization resistance of these materials.

The insights gained by the machine learning model apply specifically to pyrochlores and, because of the interpolative nature of these models, to the families of pyrochlores considered here. That said, the features identified as being best able to predict T_C can be justified physically and thus may be applicable to other classes of complex oxides, such as δ-phase,[46] that have fluorite as the parent structure. However, other classes of complex oxides, such as spinel, which have fundamentally different crystal structures, may have different dependencies on these features, or require new features to predict behavior. In particular, structural vacancies on the cation sublattice in spinel can facilitate recovery of damage in a way that is not possible in pyrochlore.[44] Further, other factors,

DOI: 10.1021/acs.chemmater.6b04666
Chem. Mater. 2017, 29, 2574−2583

such as short-range order, which is known to occur in complex oxides,[47,48] may also play a role. However, we suspect that treating the disordered state as truly random captures much of the behavior of these materials, given the ability of the disordered fluorite structure to predict order−disorder temperatures in these systems.[25,49]

In this work, we have used T_C as a metric for relative amorphization resistance. In reality, the value of T_C encompasses not only thermodynamic properties such as disordering and amorphization energetics, but also kinetic processes of defect annihilation and defect production. Further, T_C depends on irradiation conditions,[50] changing with ion mass, energy, and flux. For example, $Nd_2Zr_2O_7$ cannot be amorphized via light ion irradiations but is easily amorphized under irradiation with heavy ions.[9,51] Also, while there is a clear dependence of T_C with chemistry under 1 MeV Kr irradiations (Figure 1), irradiations with Bi and Au do not reveal such a dependence.[52,53] These observations further reinforce the fact that T_C is not an intrinsic property of a material, but is very sensitive to the irradiation conditions. Thus, actually predicting T_C from fundamental defect behavior would be a daunting task, as the computational materials modeling community cannot predict the damage state induced by arbitrary irradiation conditions nor the behavior of defects in pyrochlore as a function of disorder (further, for quantitative predictions, these quantities would need to be known at a DFT level). However, T_C does provide a metric to compare the susceptibility of amorphization that has been measured for a range of pyrochlore chemistries. In addition, while T_C will change with irradiation conditions, we expect that the general trends exhibited between different pyrochlore chemistries will not. If the trends were very sensitive to the irradiation conditions, then correlations of T_C with, e.g., disordering tendencies would not exist, as even trends in T_C would be dominated by external factors. Finally, this work demonstrates an alternative route to developing predictive models of fundamentally complicated properties such as T_C. In principle, with more experimental data, irradiation conditions could be accounted for in the machine learning model via parameters such as ion mass, energy, and flux. While a machine learning model does not provide the intuitive physical picture that a fundamental model would, it does allow for predictions of systems where developing a fundamental model is prohibitive.

Amorphization in materials such as pyrochlore is the result of one of two mechanisms.[21,54] Under light ion irradiation, defects are produced and accumulate in the material. At some defect concentration, the stored energy in the lattice is greater than that of the amorphous phase, and the material succumbs to an amorphization transformation. In some sense, this is similar to walking up the temperature axis of the phase diagram for the material, starting from a low temperature.[7] Alternatively, under heavy ion irradiation, the material is effectively melted at a local level and then solidifies. This so-called direct impact mechanism leads to direct amorphization within each damage event or collision cascade and is similar to walking down the temperature axis, starting from a very high temperature. These are qualitatively different amorphization mechanisms. Note that the dense cascades induced by the heavier ions are still within the ballistic regime and are not within a regime described by ionizing thermal spikes induced by swift heavy ions.[55] Still, dense cascades are characterized by a local thermal spike-like process, as has been demonstrated by multiple molecular dynamics simulations.[56,57] The 1 MeV Kr irradiations summarized in Figure 1 are representative of the defect accumulation mechanism, particularly in the manner in which they were performed, in which the ions went all the way through the material. However, other irradiation conditions, such as using heavier Bi or Au[52,53] ions, are better described by the direct impact mechanism and lead to qualitatively different behavior. Our results apply only to irradiation conditions in which amorphization proceeds via defect accumulation.

Returning to the nature of T_C, we have used static properties (the energetics of different pyrochlore structures and phases) to analyze an inherently kinetic quantity. However, these are not fully decoupled effects. As stated by the Bell−Evans−Polanyi principle,[42,43] the kinetics of a process is related to the difference in enthalpy between the initial and final states. Thus, there is, at least in a broad sense, a direct connection between the differences in energetics between states and the kinetic processes associated with them. In the case of pyrochlore, if the energy of the amorphous phase is high, there will be a larger driving force to recrystallize, and the kinetics associated with recrystallization will thus be faster. While this argument does not provide a quantitative link between the thermodynamics and kinetics of the various phases of the material, it does suggest that the two are not completely independent and that these thermodynamic quantities can be used as a surrogate for more complex (and unknown) kinetic quantities. Indeed, the kinetic stability of cation interstitials has been linked to the cation radii,[58] further supporting this concept.

Finally, this work highlights the utility of machine learning approaches in materials science. In this case, the ML model elucidates those features which provide predictive capability, providing insight into those factors which dictate amorphization resistance in pyrochlores. The model also shows that sets of two features result in optimal predictions; higher-order feature sets do not add significant value. The fact that different combinations of features prove optimal for describing the entire set of pyrochlores (r_A/r_B and ΔX) versus the Ti family (r_A/r_B or $E_{O\rightarrow D}$ and $E_{D\rightarrow A}$) reinforces the point that the best set of features depends on the level of detail (here, the error in the predicted T_C) required in the prediction.

■ ASSOCIATED CONTENT

Supporting Information

The Supporting Information is available free of charge on the ACS Publications website at DOI: 10.1021/acs.chemmater.6b04666.

Full five-feature data set used to develop the kernel ridge regression machine learning model (PDF)

■ AUTHOR INFORMATION

Corresponding Author

*E-mail: blas@lanl.gov.

ORCID

Karl R. Whittle: 0000-0002-8000-0857

Blas Pedro Uberuaga: 0000-0001-6934-6219

Notes

The authors declare no competing financial interest.

■ ACKNOWLEDGMENTS

This work was supported by the U.S. Department of Energy, Office of Science, Basic Energy Sciences, Materials Sciences and Engineering Division. K.R.W. and R.W.G. acknowledge funding

DOI: 10.1021/acs.chemmater.6b04666
Chem. Mater. 2017, 29, 2574−2583

from the UK's Engineering and Physical Sciences Research Council (EPSRC) under grants EP/L005581/1 and EP/L006170/1. Los Alamos National Laboratory, an affirmative action equal opportunity employer, is operated by Los Alamos National Security, LLC, for the National Nuclear Security Administration of the U.S. DOE under Contract DE-AC52-06NA25396.

REFERENCES

(1) Sickafus, K. E.; Minervini, L.; Grimes, R. W.; Valdez, J. A.; Ishimaru, M.; Li, F.; McClellan, K. J.; Hartmann, T. Radiation Tolerance of Complex Oxides. *Science* **2000**, *289*, 748−751.
(2) Begg, B. D.; Hess, N. J.; McCready, D. E.; Thevuthasan, S.; Weber, W. J. Heavy-ion Irradiation Effects in $Gd_2(Ti_{2-x}Zr_x)O_7$ Pyrochlores. *J. Nucl. Mater.* **2001**, *289*, 188−193.
(3) Lian, J.; Wang, L.; Chen, J.; Sun, K.; Ewing, R. C.; Farmer, J. M.; Boatner, L. A. The Order-Disorder Transition in Ion-Irradiated Pyrochlore. *Acta Mater.* **2003**, *51*, 1493−1502.
(4) Lian, J.; Chen, J.; Wang, L. M.; Ewing, R. C.; Farmer, J. M.; Boatner, L. A.; Helean, K. B. Radiation-Induced Amorphization of Rare-Earth Titanate Pyrochlores. *Phys. Rev. B: Condens. Matter Mater. Phys.* **2003**, *68*, 134107.
(5) Lian, J.; Helean, K. B.; Kennedy, B. J.; Wang, L. M.; Navrotsky, A.; Ewing, R. C. Effect of structure and thermodynamic stability on the response of lanthanide stannate pyrochlores to ion beam irradiation. *J. Phys. Chem. B* **2006**, *110*, 2343−2350.
(6) Helean, K. B.; Ushakov, S. V.; Brown, C. E.; Navrotsky, A.; Lian, J.; Ewing, R. C.; Farmer, J. M.; Boatner, L. A. Formation Enthalpies of Rare Earth Titanate Pyrochlores. *J. Solid State Chem.* **2004**, *177*, 1858−1866.
(7) Sickafus, K. E.; Grimes, R. W.; Valdez, J. A.; Cleave, A.; Tang, M.; Ishimaru, M.; Corish, S. M.; Stanek, C. R.; Uberuaga, B. P. Radiation-Induced Amorphization Resistance and Radiation Tolerance in Structurally Related Oxides. *Nat. Mater.* **2007**, *6*, 217−223.
(8) Lumpkin, G. R.; Pruneda, M.; Rios, S.; Smith, K. L.; Trachenko, K.; Whittle, K. R.; Zaluzec, N. J. Nature of the Chemical Bond and Prediction of Radiation Tolerance in Pyrochlore and Defect Fluorite Compounds. *J. Solid State Chem.* **2007**, *180*, 1512−1518.
(9) Sattonnay, G.; Sellami, N.; Thomé, L.; Legros, C.; Grygiel, C.; Monnet, I.; Jagielski, J.; Jozwik-Biala, I.; Simon, P. Structural Stability of $Nd_2Zr_2O_7$ Pyrochlore Ion-Irradiated in a Broad Energy Range. *Acta Mater.* **2013**, *61*, 6492−6505.
(10) Li, Y. H.; et al. Role of Antisite Disorder on Preamorphization Swelling in Titanate Pyrochlores. *Phys. Rev. Lett.* **2012**, *108*, 195504.
(11) Ringwood, A.; Kesson, S.; Ware, N.; Hibberson, W.; Major, A. *Nature* **1979**, *278*, 219.
(12) Ewing, R. C.; Lian, J.; Wang, L. M. Ion Beam-Induced Amorphization of the Pyrochlore Structure-Type: A Review. *MRS Online Proc. Libr.* **2003**, *792*, 37−48.
(13) Lumpkin, G. R.; Whittle, K. R.; Rios, S.; Smith, K. L.; Zaluzec, N. J. Temperature Dependence of Ion Irradiation Damage in the Pyrochlores $La_2Zr_2O_7$ and $La_2Hf_2O_7$. *J. Phys.: Condens. Matter* **2004**, *16*, 8557−8570.
(14) Lumpkin, G. R.; Smith, K. L.; Blackford, M. G.; Whittle, K. R.; Harvey, E. J.; Redfern, S. A. T.; Zaluzec, N. J. Ion Irradiation of Ternary Pyrochlore Oxides. *Chem. Mater.* **2009**, *21*, 2746−2754.
(15) Whittle, K. R.; Blackford, M. G.; Aughterson, R. D.; Lumpkin, G. R.; Zaluzec, N. J. Ion Irradiation of Novel Yttrium/Ytterbium-Based Pyrochlores: The Effect of Disorder. *Acta Mater.* **2011**, *59*, 7530−7537.
(16) Lian, J.; Ewing, R. C.; Wang, L. M.; Helean, K. B. Ion-Beam Irradiation of $Gd_2Sn_2O_7$ and $Gd_2Hf_2O_7$ Pyrochlore: Bond-Type Effect. *J. Mater. Res.* **2004**, *19*, 1575−1580.
(17) Meldrum, A.; Boatner, L. A.; Weber, W. J.; Ewing, R. C. Amorphization and Recrystallization of the ABO(3) Oxides. *J. Nucl. Mater.* **2002**, *300*, 242−254.
(18) Helean, K. B.; Navrotsky, A.; Lian, J.; Ewing, R. C. Correlation of Formation Enthalpies with Critical Amorphization Temperature for Pyrochlore and Monazite. *MRS Online Proc. Libr.* **2004**, *824*, 22−27.
(19) Minervini, L.; Grimes, R. W.; Sickafus, K. E. Disorder in Pyrochlore Oxides. *J. Am. Ceram. Soc.* **2000**, *83*, 1873−1878.
(20) Naguib, H. M.; Kelly, R. Criteria for Bombardment-Induced Structural Changes in Non-Metallic Solids. *Radiat. Eff.* **1975**, *25*, 1−12.
(21) Sickafus, K. E. Introducton to Mathematical Models for Irradiation-Induced Phase Transformations. In *Radiation Effects in Solids*; Springer, 2007; pp 321−352.
(22) Kresse, G.; Joubert, D. From Ultrasoft Pseudopotentials to the Projector Augmented-Wave Method. *Phys. Rev. B: Condens. Matter Mater. Phys.* **1999**, *59*, 1758−1775.
(23) Kresse, G.; Furthmuller, J. Efficient iterative schemes for ab initio total-energy calculations using a plane-wave basis set. *Phys. Rev. B: Condens. Matter Mater. Phys.* **1996**, *54*, 11169−11186.
(24) Zunger, A.; Wei, S. H.; Ferreira, L. G.; Bernard, J. E. Special Quasirandom Structures. *Phys. Rev. Lett.* **1990**, *65*, 353−356.
(25) Jiang, C.; Stanek, C. R.; Sickafus, K. E.; Uberuaga, B. P. First-Principles Prediction of Disordering Tendencies in Pyrochlore Oxides. *Phys. Rev. B: Condens. Matter Mater. Phys.* **2009**, *79*, 104203.
(26) Pedregosa, F.; et al. Scikit-learn: Machine Learning in Python. *J. Mach. Learn. Res.* **2011**, *12*, 2825−2830.
(27) Rupp, M.; Tkatchenko, A.; Muller, K.-R.; von Lilienfeld, O. A. Fast and Accurate Modeling of Molecular Atomization Energies with Machine Learning. *Phys. Rev. Lett.* **2012**, *108*, 058301.
(28) Huan, T. D.; Mannodi-Kanakkithodi, A.; Ramprasad, R. Accelerated Materials Property Predictions and Design Using Motif-Based Fingerprints. *Phys. Rev. B: Condens. Matter Mater. Phys.* **2015**, *92*, 014106.
(29) Pilania, G.; Wang, C.; Jiang, X.; Rajasekaran, S.; Ramprasad, R. Accelerating Materials Property Predictions Using Machine Learning. *Sci. Rep.* **2013**, *3*, 2810.
(30) Mannodi-Kanakkithodi, A.; Pilania, G.; Huan, T. D.; Lookman, T.; Ramprasad, R. Machine Learning Strategy for Accelerated Design of Polymer Dielectrics. *Sci. Rep.* **2016**, *6*, 20952.
(31) Botu, V.; Ramprasad, R. Adaptive Machine Learning Framework to Accelerate Ab Initio Molecular Dynamics. *Int. J. Quantum Chem.* **2015**, *115*, 1074.
(32) Botu, V.; Ramprasad, R. Learning Scheme to Predict Atomic Forces and Accelerate Materials Simulations. *Phys. Rev. B: Condens. Matter Mater. Phys.* **2015**, *92*, 094306.
(33) Ghiringhelli, L. M.; Vybiral, J.; Levchenko, S. V.; Draxl, C.; Scheffler, M. Big Data of Materials Science: Critical Role of the Descriptor. *Phys. Rev. Lett.* **2015**, *114*, 105503.
(34) Kim, C.; Pilania, G.; Ramprasad, R. From Organized High-throughput Data to Phenomenological Theory using Machine Learning: The Example of Dielectric Breakdown. *Chem. Mater.* **2016**, *28*, 1304.
(35) Kim, C.; Pilania, G.; Ramprasad, R. Machine Learning Assisted Predictions of Intrinsic Dielectric Breakdown Strength of ABX_3 Perovskites. *J. Phys. Chem. C* **2016**, *120*, 14575.
(36) Snyder, J. C.; Rupp, M.; Hansen, K.; Muller, K. R.; Burke, K. Finding Density Functionals with Machine Learning. *Phys. Rev. Lett.* **2012**, *108*, 253002.
(37) Pilania, G.; Mannodi-Kanakkithodi, A.; Uberuaga, B. P.; Ramprasad, R.; Gubernatis, J. E.; Lookman, T. Machine Learning Bandgaps of Double Perovskites. *Sci. Rep.* **2016**, *6*, 19375.
(38) Xue, D.; Balachandran, P. V.; Hogden, J.; Theiler, J.; Xue, D.; Lookman, T. Accelerated search for materials with targeted properties by adaptive design. *Nat. Commun.* **2016**, *7*, 11241.
(39) Witten, I. H.; Frank, E.; Hall, M. A. *Data Mining: Practical Machine Learning Tools and Techniques*; Elsevier, 2011.
(40) Müller, K. R.; Mika, S.; Ratsch, G.; Tsuda, K.; Scholkopf, B. An Introduction to Kernel-based Learning Algorithms. *IEEE Trans. Neural Networks* **2001**, *12*, 181−201.
(41) Hofmann, T.; Scholkopf, B.; Smola, A. J. Kernel Methods in Machine Learning. *Ann. Statist.* **2008**, *36*, 1171−1220.

DOI: 10.1021/acs.chemmater.6b04666
Chem. Mater. 2017, 29, 2574−2583

(42) Bell, R. P. The Theory of Reactions Involving Proton Transfers. *Proc. R. Soc. London, Ser. A* **1936**, *154*, 414−429.
(43) Evans, M. G.; Polanyi, M. Further Considerations on the Thermodynamics of Chemical Equilibria and Reaction Rates. *Trans. Faraday Soc.* **1936**, *32*, 1333−1360.
(44) Uberuaga, B. P.; Tang, M.; Jiang, C.; Valdez, J. A.; Smith, R.; Wang, Y.-Q.; Sickafus, K. E. Opposite Correlations Between Cation Disordering and Amorphization Resistance in Spinels Versus Pyrochlores. *Nat. Commun.* **2015**, *6*, 8750.
(45) Tracy, C. L.; Shamblin, J.; Park, S.; Zhang, F.; Trautmann, C.; Lang, M.; Ewing, R. C. Role of composition, bond covalency, and short-range order in the disordering of stannate pyrochlores by swift heavy ion irradiation. *Phys. Rev. B: Condens. Matter Mater. Phys.* **2016**, *94*, 064102.
(46) Stanek, C. R.; Jiang, C.; Uberuaga, B. P.; Sickafus, K. E.; Cleave, A. R.; Grimes, R. W. Predicted Structure and Stability of $A_4B_3O_{12}$ δ-Phase Compositions. *Phys. Rev. B: Condens. Matter Mater. Phys.* **2009**, *80*, 174101.
(47) Jiang, C.; Sickafus, K. E.; Stanek, C. R.; Rudin, S. P.; Uberuaga, B. P. Cation Disorder in MgX_2O_4 (X = Al, Ga, In) Spinels from First Principles. *Phys. Rev. B: Condens. Matter Mater. Phys.* **2012**, *86*, 024203.
(48) Shamblin, J.; Feygenson, M.; Neuefeind, J.; Tracy, C. L.; Zhang, F.; Finkeldei, S.; Bosbach, D.; Zhou, H.; Ewing, R. C.; Lang, M. Probing Disorder in Isometric Pyrochlore and Related Complex Oxides. *Nat. Mater.* **2016**, *15*, 507.
(49) Li, Y.; Kowalski, P. M.; Beridze, G.; Birnie, A. R.; Finkeldei, S.; Bosbach, D. Defect Formation Energies in $A_2B_2O_7$ Pyrochlores. *Scr. Mater.* **2015**, *107*, 18−21.
(50) Wang, S. X.; Wang, L. M.; Ewing, R. C.; Was, G. S.; Lumpkin, G. R. Ion Irradiation-Induced Phase Transformation of Pyrochlore and Zirconolite. *Nucl. Instrum. Methods Phys. Res., Sect. B* **1999**, *148*, 704.
(51) Patel, M. K.; Vijayakumar, V.; Kailas, S.; Avasthi, D. K.; Pivin, J. C.; Tyagi, A. K. Structural Modifications in Pyrochlores Caused by Ions in the Electronic Stopping Regime. *J. Nucl. Mater.* **2008**, *380*, 93−98.
(52) Begg, B. D.; Hess, N. J.; Weber, W. J.; Devanathan, R.; Icenhower, J. P.; Thevuthasan, S.; McGrail, B. P. Heavy-Ion Irradiation Effects on Structures and Acid Dissolution of Pyrochlores. *J. Nucl. Mater.* **2001**, *288*, 208−216.
(53) Ewing, R. C.; Weber, W. J.; Lian, J. Nuclear Waste Disposal - Pyrochlore ($A_2B_2O_7$): Nuclear Waste Form for the Immobilization of Plutonium and Minor Actinides. *J. Appl. Phys.* **2004**, *95*, 5949−5971.
(54) Soulié, A.; Menut, D.; Crocombette, J.-P.; Chartier, A.; Sellami, N.; Sattonnay, G.; Monnet, I.; Béchade, J.-L. X-ray Diffraction Study of the $Y_2Ti_2O_7$ Pyrochlore Disordering Sequence Under Irradiation. *J. Nucl. Mater.* **2016**, *480*, 314.
(55) Toulemonde, M.; Paumier, E.; Dufour, C. Thermal spike model in the electronic stopping power regime. *Radiat. Eff. Defects Solids* **1993**, *126*, 201−206.
(56) de la Rubia, T. D.; Averback, R.; Hsieh, H.; Benedek, R. Molecular dynamics simulation of displacement cascades in Cu and Ni: Thermal spike behavior. *J. Mater. Res.* **1989**, *4*, 579−586.
(57) Marks, N.; Thomas, B.; Smith, K.; Lumpkin, G. Thermal spike recrystallisation: Molecular dynamics simulation of radiation damage in polymorphs of titania. *Nucl. Instrum. Methods Phys. Res., Sect. B* **2008**, *266*, 2665−2670.
(58) Chartier, A.; Catillon, G.; Crocombette, J.-P. Key role of the cation interstitial structure in the radiation resistance of pyrochlores. *Phys. Rev. Lett.* **2009**, *102*, 155503.

DOI: 10.1021/acs.chemmater.6b04666
Chem. Mater. 2017, 29, 2574−2583